Superfluid Density and Collective Modes of Fermion Superfluid in Dice Lattice

Yu-Rong Wu
Guangzhou University
Xiao-Fei Zhang
Chinese Academy of Sciences
Chao-Fei Liu
Jiangxi University of Technology
Wu-Ming Liu
Chinese Academy of Sciences
Yi-Cai Zhang (zhangyicai123456@163.com)
Guangzhou University

Research Article

Keywords: Hubbard model, dice , flat band, counterparts , superconductor

Posted Date: April 15th, 2021

DOI: https://doi.org/10.21203/rs.3.rs-418100/v1

Superfluid density and collective modes of fermion superfluid in dice lattice

Yu-Rong Wu[1], Xiao-Fei Zhang[2,3], Chao-Fei Liu[4], Wu-Ming Liu[5,6], and Yi-Cai Zhang[1*]

[1]School of Physics and Materials Science, Guangzhou University, Guangzhou 510006, People's Republic of China
[2]Key Laboratory of Time and Frequency Primary Standards, National Time Service Center, Chinese Academy of Sciences, Xi'an 710600, China
[3]School of Astronomy and Space Science, University of Chinese Academy of Sciences, Beijing 100049, China
[4]School of Science, Jiangxi University of Technology, Ganzhou, 341000, China
[5]Beijing National Laboratory for Condensed Matter Physics, Institute of Physics, Chinese Academy of Sciences, Beijing 100190, China
[6]Songshan Lake Materials Laboratory, Dongguan, Guangdong 523808, China
[*]zhangyicai123456@163.com

ABSTRACT

The superfluid properties of attractive Hubbard model in dice lattice are investigated. It is found that three superfluid order parameters increase as the interaction increases. When the filling factor falls into the flat band, due to the infinite large density of states, the resulting superfluid order parameters are proportional to interaction strength, which is in striking contrast with the exponentially small counterparts in usual superfluid (or superconductor). When the interaction is weak and the filling factor is near the bottom of lowest band (or the top of highest band), the superfluid density is determined by the effective mass of the lowest (or highest) single-particle band. When the interactions is strong and filling factor is small, the superfluid density is inversely proportional to interaction strength, which is related to effective mass of tightly bound pairs. In the strong interaction limit and finite filling, the asymptotic behaviors of superfluid density can be captured by a parabolic function of filling factor. Further more, when the filling is in flat band, the superfluid density shows a logarithmic singularity as the interaction approaches zero. In addition, there exist three undamped collective modes for strong interactions. The lowest excitation is gapless phonon, which is characterized by the total density oscillations. The two others are gapped Leggett modes, which correspond relative density fluctuations between sublattices. The collective modes are also reflected in the two-particle spectral functions by sharp peaks. Further more, it is found that the two-particle spectral functions satisfy an exact sum-rule, which is directly related to the filling factor (or density of particle). The sum-rule of the spectral functions may be useful to distinguish the hole-doped or particle-doped superfluid (superconductor) in experiments.

Introduction

The superfluid properties in multi-component (or multi-band) system have been attracting a great interests[1–3]. In comparing with single-component superfluid counterpart, a lot of novel physics, for example, existence of gapped Leggett modes[4–8], color superconductor[9–11], coexistence of superfluid and ferromagnetic polarizations[12,13], induced effective interaction[14], breaking of Galilean invariance in spin-orbit coupled Bose-Einstein condensation (BEC)[15], etc, in multi-component superfluid would appear.

For a single flat band system, due to divergence of effective mass[16], it is believed that the flat system usually has no superfluidity, e.g., the superfluid density (which is superfluid weight up to a constant) $\rho_s = 0$. However, for a multi-band system, the situation may be quite different[17,18]. In contrast to the single-band system, the superfluid density in a multi-band system can be divided into two part contributions. One of that consists of the diagonal matrix elements of current operator (conventional part), and the other one is the off-diagonal terms (the so called geometric part[19–21]). Even through the conventional part may vanish in flat band limit, the geometric one may be finite. Furthermore, it is found that under some conditions, the geometric part of superfluid density is related to the geometric quantity of energy band, namely, the geometric metric tensor of Bloch states[22].

The flat band can appear in dice (T_3) lattice, similar as graphene, which also has the honeycomb lattice structure (see Fig. 1). In comparing with the graphene, there is an extra lattice site (per unit cell) in the center of hexagon of honeycomb lattice[23–25]. The low-energy physics of the dice lattice are also described by the Dirac equation, but its pseudospin $S = 1$ instead of $\frac{1}{2}$[26,27]. There are two schemes to obtain this kind of lattice: one is to fabricate the trilayer structure of cubic lattice (e.g.$SrTiO_3/SrIrO_3/SrTiO_3$) in the (111) direction[28], and the other one is to use the cold atoms in the optical lattice[29]. The

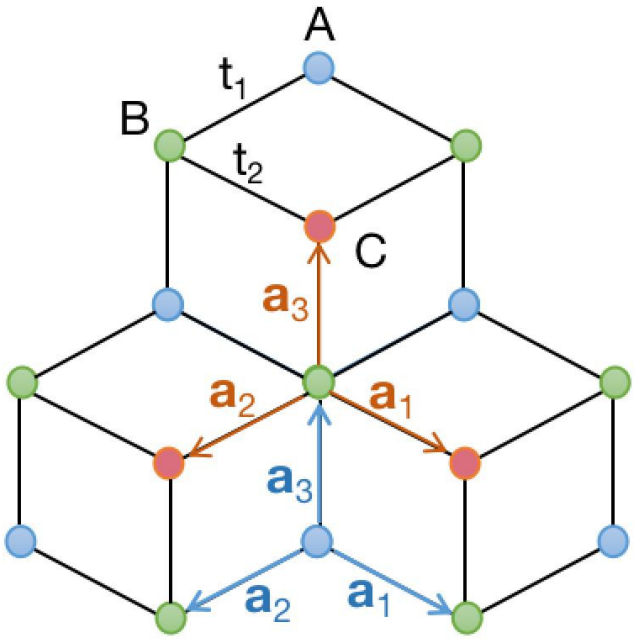

Figure 1. The structure of dice lattice. Sublattices A, B and C are shown in blue, green and red respectively. The vectors $\mathbf{a}_1 = [\sqrt{3}/2, -1/2]$, $\mathbf{a}_2 = [-\sqrt{3}/2, -1/2]$ and $\mathbf{a}_3 = [0, 1]$ with lattice spacing $a \equiv 1$.

band structure of the dice lattice has a distinguishing characteristic compared to the graphene, in addition to the conduction band and valence band $E_{\pm}(k)$, there is a flat band $E_0(k)$ in the middle. For highest (or lowest) band in the Brillouin Zone, there exists two Dirac points, which closely attach to the flat band. Following the discovery of this new material, a lot of novel physical phenomena, for example, Hofstadter butterfly effect[30], magneto-optical conductivity[31], Super-Klein tunneling[32], zitterbewegung effect[33], magnetism[34], and magnetoconductivity[35,36], etc., have attracted great interests.

Although the superfluid density in three band Lieb lattice has been studied[17], there are still other open questions worthwhile to investigate. For example, what roles does the effective mass play in superfluidity? How do the flat band and Dirac point affect the superfluid order parameters and superfluid density? The collective modes are also interesting subjects in such a three band system. There usually exists several superfluid order parameters in multi-band system. The oscillations between different order parameters result in the so-called Leggett modes[4]. The Leggett modes in condensed system have been observed experimentally in multi-band superconductor MgB_2, by using Raman spectroscopy[37], by angle-resolved photoemission spectroscopy[38]. For three band superfluid in dice lattice, it is expected there may exist several Leggett modes.

In this work, we study the superfluid properties and collective modes of attractive Hubbard model in dice lattice. It is found that the flat band has important influences on the superfluid order parameters and superfluid density. In addition, there exists three collective modes, one of that is the gapless phonon mode, the other two are gapped Leggett modes. The collective modes can be reflected by sharp peaks in two-particle spectral functions. Futhermore, an exact sum-rule of spectral functions is derived, which may be useful to distinguish the hole-doped or particle-doped superfluid (or superconductor) in experiments.

Results

The structure of dice lattice is depicted in Fig.1, every unit cell consists of three different lattice sites (A,B and C), in which sites A and B are located at the vertices of hexagonal to form honeycomb lattice, and site C is located at the center of the hexagon. In this work, we only consider the nearest neighbor hopping and equal hopping amplitude, i.e., $t_1 = t_2 = t$ (see Fig. 1). The Hubbard model in which two-component Fermi gases with spin $\sigma = \uparrow, \downarrow$ interacting through on-site attractive interaction $-U$ ($U > 0$) is

$$\mathscr{H} = \sum_{\langle ij\rangle\sigma} t_{ij} c^{\dagger}_{i\sigma} c_{j\sigma} - \mu \sum_{i\sigma} n_{i\sigma} - U \sum_{i} n_{i\uparrow} n_{i\downarrow}, \tag{1}$$

where μ describes the chemical potential. In the following, we would use i to label the unit cell. The creation operators for three sub-lattices are represented by $a^{\dagger}_i$, $b^{\dagger}_i$ and $c^{\dagger}_i$ respectively. $n_{i\sigma} = c^{\dagger}_{i\sigma} c_{i\sigma}$ is the particle number operator. Under periodic

boundary condition , using the Fourier transform, it is convenient to obtain the non-interacting Hamiltonian

$$\mathscr{H}_0(\mathbf{k}) = \sum_{\sigma} \psi_{\sigma}^{\dagger}(\mathbf{k}) h(\mathbf{k}) \psi_{\sigma}(\mathbf{k}), \tag{2}$$

with $\psi_{\sigma}^{\dagger}(\mathbf{k}) = [a_{\sigma}^{\dagger}(\mathbf{k}), b_{\sigma}^{\dagger}(\mathbf{k}), c_{\sigma}^{\dagger}(\mathbf{k})]$ and

$$h(\mathbf{k}) = \begin{bmatrix} M-\mu & h_{12}(\mathbf{k}) & 0 \\ h_{21}(\mathbf{k}) & -\mu & h_{23}(\mathbf{k}) \\ 0 & h_{32}(\mathbf{k}) & -M-\mu \end{bmatrix} \tag{3}$$

where $h_{12}(\mathbf{k}) = t\sum_{\delta}\cos(\mathbf{k}\cdot\mathbf{a}_{\delta}) + it\sum_{\delta}\sin(\mathbf{k}\cdot\mathbf{a}_{\delta})$, $h_{21}(\mathbf{k}) = h_{12}^{*}(\mathbf{k})$, $h_{23}(\mathbf{k}) = h_{12}(\mathbf{k})$, $h_{32}(\mathbf{k}) = h_{21}(\mathbf{k})$, and $\mathbf{k} = (k_x, k_y)$. The two dimensional vectors $\mathbf{a}_{\delta}$ are shown in Fig.1. We note that it is a multi-band (three-band) system and there exist a flat band $[E_0 = 0]$ in between highest $[E_+(k)]$ and lowest bands $[E_-(k) = -E_+(k)]$.

It is worthy noting that the important roles played by particle-hole symmetry in this model. Similarly as Haldane-Hubbard model[39], applying particle-hole transformation to the system,

$$c_{i\sigma} \to \varepsilon_i c_{i\sigma}^{\dagger}, \;\; c_{i\sigma}^{\dagger} \to \varepsilon_i c_{i\sigma}, \tag{4}$$

where $\varepsilon_i = 1$ for the A and C sublattices, and for the B sublattices $\varepsilon_i = -1$, the hopping term in Hamiltonian Eq.(1) is invariant under the above transformation. After adding some constant terms, the interaction term remains invariant and chemical potential term changes a sign. At this point, we only need to consider the case where the number of particles $n > 3$ ($n = 3$ is half-filling, i.e. there are three particles in a unit cell). For filling $\Delta n \equiv n - 3 \geq 0$ (particle-doped case) and $-\Delta n = 3 - n \leq 0$ (hole-doped case), the chemical potentials satisfy a relationship

$$\mu(-\Delta n) = -\mu(\Delta n). \tag{5}$$

It indicates that, at half-filling ($n = 3$), the chemical potential is exactly zero. Further more, we will see that all the other physical quantities, e.g., superfluid order parameters, superfluid density, etc., are also symmetrical with respect to the half-filling $n = 3$ (see Fig. 2).

The order parameters ($\Delta_i = -U\langle c_{i\downarrow} c_{i\uparrow}\rangle$) can be calculated with mean field theory (see **Metholds**). The evolutions of the superfluid order parameters are depicted in panel (a) of Fig. 2. It is found that Δ_i is always real. The order parameters is symmetrical with respect to the half-filling due to the particle-hole symmetry. The Hamiltonian is subject to the inversion symmetry, Δ_A is the same as Δ_C but differ from ΔB. As one increases the interaction U, Δ_i always increases. The order parameters can increase without limit as long as the interaction is strong enough. For example, when filling factor is half-filling ($n = 3$), $\Delta_i \simeq U/2$ as $U \to \infty$, which is the half of the energy of two particle bound states[40].

When the filling factor approaches zero, the order parameters decrease to zero. The fully occupied case ($n = 6$) is equivalent to completely empty ($n = 0$) case due to the particle-hole symmetry. With the increasing of filling factor n, the Δ_i gets larger. However, when the filling factor is in between lowest band and middle flat band, the order parameter gets a dip due to the small density of states near the Dirac points [especially for weakly interacting cases in panel (a) of Fig.2]. The suppressions of order parameters are also found in Lieb lattice[41]. When the filling factor lies in the middle region (e.g., $n \simeq 3$), the order parameter reaches its maximum due to enhancement of density of states in flat band.

The interaction effects amplified by band flatness can give rise to Wigner-crystal state[42] and ferromagnetic transition[43]. Similarly, the behaviors of superfluid order parameters are also affected significantly by the flat band[44]. For example, when the filling factor is in middle of the flat band (e.g., half filling $n = 3$), the infinite large density of states results in order parameter $\Delta_A = \Delta_C \simeq U/4$ as the interaction approaches zero, which is very different from that in the usual Bardeen-Cooper-Schrieffer (BCS) superconductor (or superfluid), where pairing gap Δ is exponentially small when interaction $U \to 0$. In addition, it is found that the order parameter for sublattice B is much smaller than $\Delta_{A(C)}$ when the interaction is small ($U/t \ll 1$), i.e., $\Delta_B/\Delta_{A(C)} \ll 1$.

Superfluid density

The superfluid density can be calculated with phase twist method[19,45]. Assuming the superfluid order parameters undergo a phase variation, e.g, $\triangle_i \to \Delta_i e^{2i\mathbf{q}\cdot\mathbf{r}_i}$, the superfluid density (particle number per unit cell) tensor ρ_{sij} can be written as

$$\rho_{sij} = \frac{\partial^2 \Omega(\mathbf{q})}{\partial q_i \partial q_i}|_{q\to 0}, \tag{6}$$

where Ω is thermodynamical potential (per unit cell) in grand canonical ensemble. Similarly as the Haldane model[19], due to the C_3 symmetry of honeycomb lattice[18,46], the superfluid density tensor can be simplified into a scalar, i.e., $\rho_{sij} = diag\{\rho_s, \rho_s\}$.

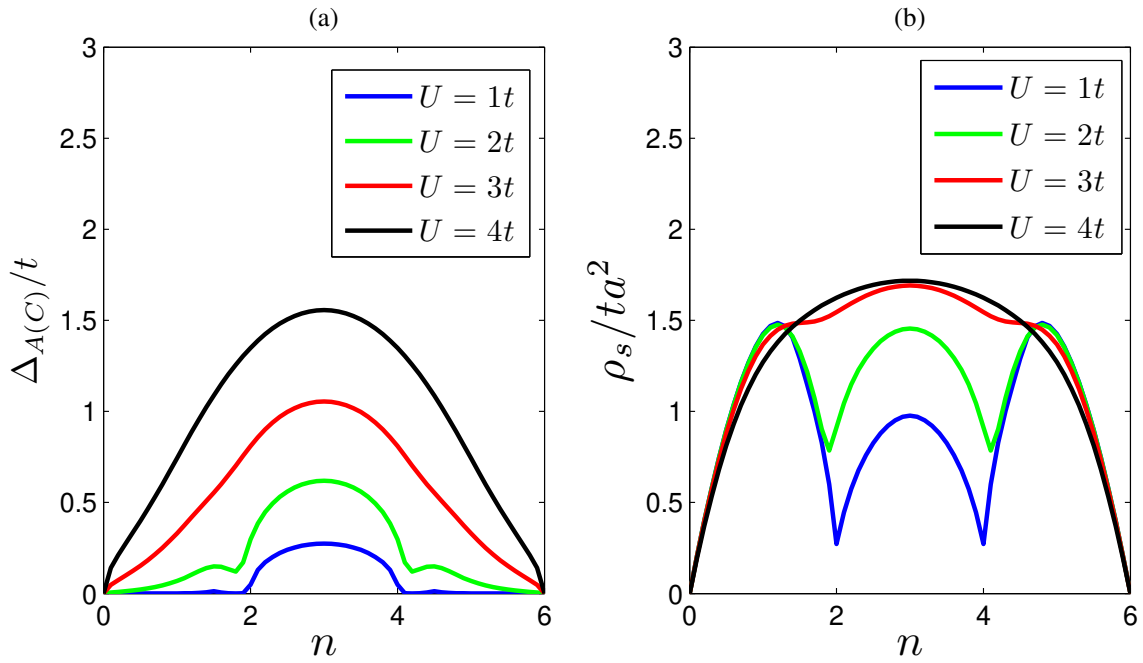

Figure 2. The superfluid order parameters for sublattice A(C) and superfluid densities as functions of filling factor n. (a): The superfluid order parameters for interaction $U = 1$, $U = 2$, $U = 3$ and $U = 4$ are shown in blue, green, red and black lines, respectively. (b): The superfluid densities for interaction $U = 1$, $U = 2$, $U = 3$ and $U = 4$ are also shown in blue, green, red and black lines, respectively.

The superfluid density ρ_s is plotted as a function of filling factor for different interactions in panel (b) of Fig. 2. First of all, we see that the superfluid density is also symmetrical with respect to half-filling due to the particle-hole symmetry. When the filling factor approaches the empty ($n \to 0$) or fully occupied cases ($n \to 6$), the superfluid density vanishes linearly. For the small filling factor case ($n \ll 1$) and weak interaction $U \ll t$ (BCS-limit[47]), the superfluid density can be written as

$$\rho_s(U/t \ll 1) = n/m^* = 3tn/(\sqrt{2}) \simeq 2.12nt, \tag{7}$$

where $m^* = \sqrt{2}/(3t)$ is the effective mass near the bottom of lowest band, which is determined by the single-particle energy band structure, and does not depend on interaction strength U. The superfluid density is proportional to filling factor (or particle density) and inversely proportional to the effective mass of energy band[16], which is very similar to that of Bose-Einstein condensate with spin-orbital coupling[48].

Differently from order parameters, when interaction $U/t \gg 1$, the superfluid density remains finite. In such case, the superfluid consists of tightly bound pairs. Two bound pairs could not occupy a same lattice site due to the constraint of exclusive principle of fermions. So the pairs can be viewed as hard core bosons, which is BEC limit of fermion superfluid. When the number of the effective hard core bosons is small $n \ll 1$ (dilute gas limit), the superfluid density is determined by the effective mass of tightly bound pairs, i.e.,

$$\rho_s(U/t \gg 1) = n'/m'^* = 8t^2 n/U, \tag{8}$$

where $n' = n/2$ is filling factor of effective hard core bosons and $m'^* = U/(16t^2)$ is its effective mass, which is determined by the dispersion of two-particle bound state energy (Note $m'^* \neq 2m^*$ due to the coupling of between the motions of center of mass and relative motion of two particles in lattice[49]). The above equation indicates that when the interaction get stronger (in strong interaction limit), the effective mass becomes larger, the resulting superfluid density gets smaller. For moderate interaction strength (e.g., $U/t > 5$), and small filling ($n \ll 1$), it is expected that the superfluid density should satisfy $8t^2 n/U < \rho_s < 2.12nt$.

In addition, differently from the order parameters, the evolution trends of superfluid density with the interactions are different for different filling factors. For example, when the filling is small, superfluid density diminishes with the increasing of interaction, which is opposite to that of order parameters [see panel (b) of Fig. 2]. Only when the filling is sufficiently large (for example, $n \simeq 3$), the superfluid density grows up as the interaction increases (within a certain range of interaction, see

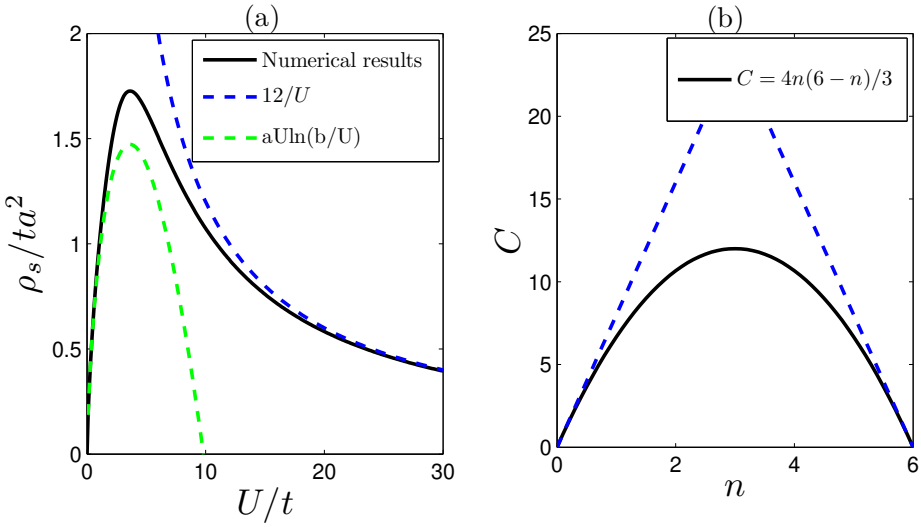

Figure 3. The asymptotic behaviors of superfluid densities. (a): The numerical results of superfluid density is plotted in black solid line (filling factor $n = 3$). The two dashed lines correspond two asymptotic limits of superfluid density, which are given by $\rho_s \simeq 12/U$ for $U \to \infty$) and $aUln(b/U)$ with $a = 0.4077$ and $b = 9.822$ for $U \to 0$, respectively. (b): The blue dashed line is the estimated up bound $8n$ (filling factor $0 \leq n \leq 3$), which is determined by effective mass of tightly bound pairs $[m^{'*} = U/(16t^2)]$. Using the particle-hole symmetry, the corresponding up bound for $3 \leq n \leq 6$ also depicted here. The solid line is the parabolic function Eq.(10).

the following discussions and the panel (a) of Fig. 3). Due to the vanishing small density of states near the Dirac points, the superfluid density also develops a dip for weak interacting cases. Similarly as Lieb lattice[17], a triple dome structure appears in the superfluid density, especially for weakly interacting cases [see panel (b) of Fig. 2].

For intermediate filling factor (e.g, $n = 3$ in flat band), it is found that the superfluid density approaches zero as $U \to 0$. Once the interaction is turned on, the superfluid density grows rapidly [see panel (a) of Fig. 3]. Specially here, the non-vanishing superfluid density for weak interactions mainly arises from the contributions of off-diagonal matrix elements of current operator (the geometric part). In the isolated flat band limit[17,21] or under the assumption of uniform pairing[1,19], the superfluid density in flat band can be related to geometric metric tensor of Bloch sates. However, here we note that the superfluid density approaches zero according to the law of

$$\rho_s = aUln[b/U], \tag{9}$$

as $U \to 0$ with two constants $a \simeq 0.4077$ and $b = 9.822$ for half filling $n = 3$ [see panel (a) in Fig.3], which is different from the linear dependence in isolated flat band limit[17]. As $U \to 0$, the appearance of the logarithmic singularity ($UlnU$) is attributed to the existences of the gapless Dirac points and vanishingly small pairing gap ($\Delta \propto U \to 0$). This is because when filling factor is in the middle of flat band (half-filling of $n = 3$) and $U \to 0$ (or $\Delta \equiv \Delta_A = \Delta_C \simeq U/4 \to 0$), it is found that the superfluid density mainly arises from matrix elements of current operator between the flat band and other bands near the Dirac points (the off-diagonal part). Further more, the contribution near the Dirac points can be approximated by $\rho_s \sim A\Delta \int_0^B \frac{qdq}{\sqrt{q^2+\Delta^2}(\sqrt{q^2+\Delta^2}+3\Delta)} = A\Delta ln\frac{\sqrt{B^2+\Delta^2}+3\Delta}{4\Delta} \simeq aUln(b/U)$, where A, B, a and b are four constants.

With the increasing of interaction, the superfluid density reaches its maximum values at $U \simeq 3.7t$ [see panel (a) in Fig.3]. After that point, it goes down. For strong interaction limit and finite n, the trend of evolutions of superfluid density can be also understood qualitatively by effective mass of tightly bound pairs. Considering the nature of fermion of tightly bound pairs, it is expected that the superfluid density should be smaller than that determined by m'^*, namely, $\rho_s < 8t^2n/U$ for BEC limit ($U \gg t$). For example, when $n = 3$, it is found that the superfluid density is also inversely proportional to interaction, i.e., $\rho_s \to C/U$ as $U \to \infty$ [see panel (a) of Fig.3]. The numerical results give the constant $C \simeq 12$ for half-filling case ($n = 3$), which is almost one half of the estimated up bound [$8t^2n = 24$ (t=1)]. Nevertheless, the up bound would provide much more precise estimation for superfluid density when filling factor n is small [see panel (b) of Fig.3]. For a general filling n, it is found that the constant

C can be given by a parabolic function, namely

$$C = \frac{4t^2}{3} n(6-n). \tag{10}$$

The asymptotic result Eq.(10) in strong interaction limit is very similar to the behavior of the superfluid density of hard core bosons in lattice[50,51].

Collective modes

In this section, we would present Gaussian fluctuation method[52–54] to calculate the collective modes and spectral functions[39]. The order parameters can be decomposed as mean-field part and fluctuation, i.e., $\Delta_i = \Delta_i + \delta\Delta_i$ with $i = 1, 2, ...m$, and m is the number of order parameters. The partition function can be written as

$$Z \approx e^{-S_0} \int D\eta_q^\dagger D\eta_q e^{-\delta S}, \tag{11}$$

where S_0 is the mean-field contribution and the Gaussian fluctuation part

$$\delta S = \tfrac{1}{2} \textstyle\sum_{\mathbf{q},n} \eta_q^\dagger M(q) \eta_q = \sum_{\mathbf{q},n>0} \eta_q^\dagger M(q) \eta_q, \tag{12}$$

with pairing fluctuation fields $\eta_q^\dagger = [\Delta_{1q}^*, \Delta_{2q}^*, ..., \Delta_{mq}^*, \Delta_{1,-q}, \Delta_{2,-q}, \Delta_{m,-q}]$ and $q = (\mathbf{q}, i\omega_n)$, $\omega_n = 2n\pi/\beta$ ($n \in Z$) is Matsubara frequency, $\beta = 1/T$ is inverse temperature. The fluctuation matrix M is a $2m \times 2m$ matrix,

$$\begin{aligned}
M_{ij}(\mathbf{q}, i\omega_n) &= \frac{1}{\beta} \sum_{\mathbf{k},n'} G_{ij}(k+q) G_{j+m,i+m}(k) + \frac{\delta_{ij}}{U}, && (1 \le i, j \le m) \\
M_{ij}(\mathbf{q}, i\omega_n) &= \frac{1}{\beta} \sum_{\mathbf{k},n'} G_{ij}(k+q) G_{j-m,i+m}(k), && (1 \le i \le m \ \& \ m+1 \le j \le 2m) \\
M_{ij}(\mathbf{q}, i\omega_n) &= \frac{1}{\beta} \sum_{\mathbf{k},n'} G_{ij}(k+q) G_{j+m,i-m}(k), && (m+1 \le i \le 2m \ \& \ 1 \le j \le m) \\
M_{ij}(\mathbf{q}, i\omega_n) &= \frac{1}{\beta} \sum_{\mathbf{k},n'} G_{ij}(k+q) G_{j-m,i-m}(k) + \frac{\delta_{ij}}{U}, && (m+1 \le i, j \le 2m),
\end{aligned} \tag{13}$$

where

$$G_{ij}(k) = ([i\omega_{n'} - H_{\mathrm{BdG}}(\mathbf{k})]^{-1})_{ij}, \tag{14}$$

is matrix element of Nambu-Gorkov Green function. Here $k = (\mathbf{k}, i\omega_{n'})$ and $\omega_{n'} = (2n'+1)\pi/\beta$ [$n' \in Z$].

The collective modes are given by zeros of determinant $Det|M(\mathbf{q}, i\omega_n \to \omega + i0^+)| = 0$. As $q \to 0$, the gapless collective mode is the Anderson-Bogoliubov phonon, which characterizes the density oscillations of superfluid. The gapped ones are Leggett modes, which correspond relative oscillations of densities of different sublattice[4–7].

With the action δS (Gaussian weight), the correlation functions (and the matrix elements of two-particle Green functions) can be calculated[46], i.e.,

$$\begin{aligned}
-G_{II,ij}(q) &= \langle \Delta_{jq}^* \Delta_{iq} \rangle = (M^{-1})_{i,j}, \\
-F_{II,ij}(q) &= \langle \Delta_{j,-q} \Delta_{iq} \rangle = (M^{-1})_{i,m+j}, \\
-F_{II,ji}^*(q) &= \langle \Delta_{jq}^* \Delta_{i,-q}^* \rangle = (M^{-1})_{m+i,m+j}, \\
-G_{II,ji}(-q) &= \langle \Delta_{j,-q} \Delta_{i,-q}^* \rangle = (M^{-1})_{m+i,m+j}.
\end{aligned} \tag{15}$$

where indices $1 \le i, j \le m$. $G_{II,ij}(F_{II,ij})$ are the two-particle normal (anomalous) Green function matrix elements[46], i.e.,

$$\begin{aligned}
G_{II,ij}(\mathbf{q}, i\omega_n) &= \sum_n [\frac{\langle 0|\Delta_{i\mathbf{q}}|n\rangle\langle n|\Delta_{j\mathbf{q}}^\dagger|0\rangle}{i\omega_n - \omega_{n0}} - \frac{\langle 0|\Delta_{j\mathbf{q}}^\dagger|n\rangle\langle n|\Delta_{i\mathbf{q}}|0\rangle}{i\omega_n + \omega_{n0}}], \\
F_{II,ij}(\mathbf{q}, i\omega_n) &= \sum_n [\frac{\langle 0|\Delta_{j,\mathbf{q}}|n\rangle\langle n|\Delta_{i,-\mathbf{q}}|0\rangle}{i\omega_n - \omega_{n0}} - \frac{\langle 0|\Delta_{i,-\mathbf{q}}|n\rangle\langle n|\Delta_{j,\mathbf{q}}|0\rangle}{i\omega_n + \omega_{n0}}].
\end{aligned} \tag{16}$$

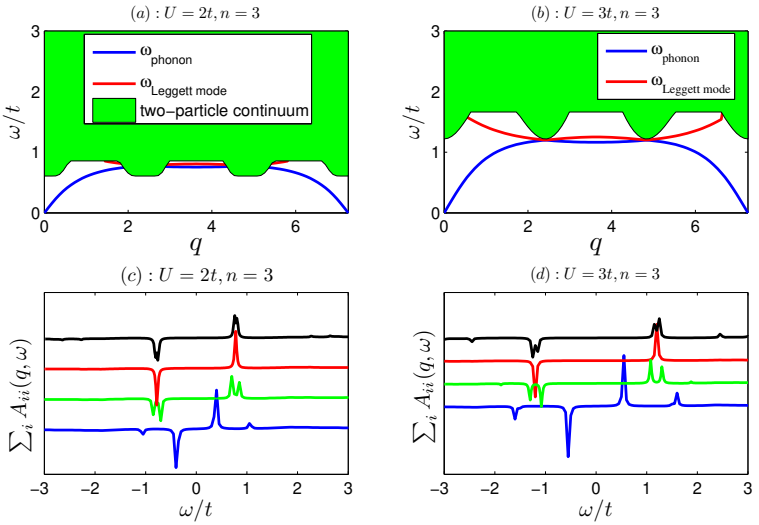

Figure 4. Collective modes [panel (a) and (b)] and two-particle spectral functions [panel (c) and (d)]. (a): The phonon (Leggett) mode is plotted in blue (red) line. The green shaded region is the two-particle continuous spectra. The interaction $U = 2$, filling factor $n = 3$ in panel (a). (b): The phonon mode and Leggett mode with $U = 3; n = 3$. (c): Spectral functions with $U = 2; n = 3$. (d): Spectral functions with $U = 3; n = 3$. The spectral functions of $q = 0.5, 1.5, 2.5$ and 3.5 are plotted in blue, green, red and black lines, respectively. The sharp peaks in spectral functions correspond the collective modes. In order to get the spectral functions numerically, we take $0^+ = 0.02$ in Eq.(17).

The two-particle spectral functions can be expressed in terms of the Green functions as[55]

$$A_{ij}(\mathbf{q},\omega) = -\frac{1}{\pi} Im[G_{II,ij}(\mathbf{q}, i\omega_n \to \omega + i0^+)]$$
$$B_{ij}(\mathbf{q},\omega) = -\frac{1}{\pi} Im[F_{II,ij}(\mathbf{q}, i\omega_n \to \omega + i0^+)], \tag{17}$$

where 0^+ denotes a positive infinitesimal number. In addition, in the presence of inversion symmetry, the superfluid density can be also related to the pairing fluctuation matrix M[46]

$$\rho_s = \lim_{q\to 0} \frac{4}{q^2} (\Delta^{t*}, \Delta^t) . \begin{pmatrix} I & 0 \\ 0 & -I \end{pmatrix} . M(q) . \begin{pmatrix} I & 0 \\ 0 & -I \end{pmatrix} . \begin{pmatrix} \Delta \\ \Delta^* \end{pmatrix} . \tag{18}$$

where $(I)_{m\times m}$ is a $m \times m$ identity matrix, $\Delta = (\Delta_1, \Delta_2, ..., \Delta_m)^t$, and $(...)^t$ denotes matrix transpose. In dice lattice case, the number of order parameters $m = 3$ and we identify $\Delta_1 = \Delta_A$, $\Delta_2 = \Delta_B$ and $\Delta_3 = \Delta_C$.

Fig. 4 and 5 show the collective modes with the increasing of wave vector q. It is found that there exist three undamped collective modes for strong interactions [see panel (a) and (b) of Fig. 5]. The lowest one is the gapless phonon as $q \to 0$, which corresponds to total density oscillation. The upper two gapped excitations are the Leggett modes, which corresponds to the relative density oscillations between sublattices. As the interaction strength decreases, the bottom of two-particle continuum lowers, the region of the existence of collective modes shrinks. The collective modes merges into the continuum and becomes damped [see panel (a) and (b) of Fig. 4]. As a result of that, the collective modes is not well defined. Only when the interaction is strong enough, the undamped Leggett modes survives (see Fig. 5). The collective modes also reflected in the two-particle spectral functions as shown in Fig. 4 and Fig. 5. The sharp peaks in spectral functions correspond the collective modes [see panel (c) and (d) in Fig. 4 and 5].

Two-particle spectral functions

The two-particle spectral functions for a general superfluid state can be also defined as

$$A_{\alpha\beta,\gamma\delta}(\mathbf{q},\omega) = \sum_n \langle 0|\Delta_{\alpha\beta\mathbf{q}}|n\rangle\langle n|\Delta^\dagger_{\gamma\delta\mathbf{q}}|0\rangle \delta(\omega - \omega_{n0}) - \sum_n \langle 0|\Delta^\dagger_{\gamma\delta\mathbf{q}}|n\rangle\langle n|\Delta_{\alpha\beta\mathbf{q}}|0\rangle \delta(\omega + \omega_{n0}),$$
$$B_{\alpha\beta,\gamma\delta}(\mathbf{q},\omega) = \sum_n \langle 0|\Delta_{\alpha\beta\mathbf{q}}|n\rangle\langle n|\Delta_{\gamma\delta,-\mathbf{q}}|0\rangle \delta(\omega - \omega_{n0}) - \sum_n \langle 0|\Delta_{\gamma\delta,-\mathbf{q}}|n\rangle\langle n|\Delta_{\alpha\beta\mathbf{q}}|0\rangle \delta(\omega + \omega_{n0}), \tag{19}$$

where $\omega_n = E_n - E_0$, E_n and $|n\rangle$ are eigenvalues and eigenstates of Hamiltonian, respectively. $\Delta_{\alpha\beta\mathbf{q}}$ is pairing fluctuation operator of superfluid order parameters, i.e.,

$$\Delta_{\alpha\beta\mathbf{q}} = -U\sum_{\mathbf{k}} c_{\alpha\mathbf{k}+\mathbf{q}} c_{\beta-\mathbf{k}}, \tag{20}$$

where $c_{\alpha\mathbf{k}+\mathbf{q}}$ fermion field operator for states in momentum space, which satisfies anti-commutation relation

$$c_{\alpha\mathbf{k}} c^{\dagger}_{\beta\mathbf{k}'} + c^{\dagger}_{\beta\mathbf{k}'} c_{\alpha\mathbf{k}} = \delta_{\alpha\beta}\delta_{\mathbf{k}\mathbf{k}'}. \tag{21}$$

The two-particle normal (anomalous) Green functions can be expressed in terms of spectral functions, i.e.,

$$\begin{aligned} G_{II\alpha\beta,\gamma\delta}(\mathbf{q}, i\omega_n) &= \int_{-\infty}^{+\infty} d\omega \frac{A_{\alpha\beta,\gamma\delta}(\mathbf{q},\omega)}{i\omega_n - \omega}, \\ F_{II\alpha\beta,\gamma\delta}(\mathbf{q}, i\omega_n) &= \int_{-\infty}^{+\infty} d\omega \frac{B_{\alpha\beta,\gamma\delta}(\mathbf{q},\omega)}{i\omega_n - \omega}. \end{aligned} \tag{22}$$

Similarly as single-particle spectral function[56], the two-particle spectral functions satisfies a sum rule, i.e.,

$$\begin{aligned} &\int d\omega A_{\alpha\beta,\gamma\delta}(\mathbf{q},\omega) = \langle 0|[\Delta_{\alpha\beta\mathbf{q}}, \Delta^{\dagger}_{\gamma\delta\mathbf{q}}]|0\rangle = U^2\langle 0|\sum_{\mathbf{k}}[\delta_{\beta\delta} c_{\alpha\mathbf{k}} c^{\dagger}_{\gamma\mathbf{k}} - \delta_{\alpha\gamma} c^{\dagger}_{\delta\mathbf{k}} c_{\beta\mathbf{k}}]|0\rangle \\ &= U^2\langle 0|\sum_{\mathbf{k}}[\delta_{\beta\delta}\delta_{\alpha\gamma} - \delta_{\beta\delta} c^{\dagger}_{\gamma\mathbf{k}} c_{\alpha\mathbf{k}} - \delta_{\alpha\gamma} c^{\dagger}_{\delta\mathbf{k}} c_{\beta\mathbf{k}}]|0\rangle, \\ &\int d\omega B_{\alpha\beta,\gamma\delta}(\mathbf{q},\omega) = \langle 0|[\Delta_{\alpha\beta\mathbf{q}}, \Delta_{\gamma\delta-\mathbf{q}}]|0\rangle = 0. \end{aligned} \tag{23}$$

Taking the diagonal elements ($\gamma = \alpha; \delta = \beta$),

$$\begin{aligned} &\int d\omega A_{\alpha\beta,\alpha\beta}(\mathbf{q},\omega) = \langle 0|[\Delta_{\alpha\beta\mathbf{q}}, \Delta^{\dagger}_{\alpha\beta\mathbf{q}}]|0\rangle = U^2\langle 0|\sum_{\mathbf{k}}[c_{\alpha\mathbf{k}} c^{\dagger}_{\alpha\mathbf{k}} - c^{\dagger}_{\beta\mathbf{k}} c_{\beta\mathbf{k}}]|0\rangle \\ &= U^2\langle 0|\sum_{\mathbf{k}}[1 - c^{\dagger}_{\alpha\mathbf{k}} c_{\alpha\mathbf{k}} - c^{\dagger}_{\beta\mathbf{k}} c_{\beta\mathbf{k}}]|0\rangle = U^2[N_{cell} - (N_\alpha + N_\beta)], \end{aligned} \tag{24}$$

where N_{cell} is the number of unit cells, N_α is the particle number of $\alpha-$th component.

In our dice lattice case, there exist three order parameters and they can be identified as $\Delta_{A(B/C)\downarrow A(B/C)\uparrow} = \Delta_{A(B/C)}$. The sum-rule is

$$\begin{aligned} &\int d\omega B_{i,j}(\mathbf{q},\omega) = \langle 0|[\Delta_{i\mathbf{q}}, \Delta_{j-\mathbf{q}}]|0\rangle = 0, \\ &\int d\omega A_{i,j}(\mathbf{q},\omega) = \langle 0|[\Delta_{i\mathbf{q}}, \Delta^{\dagger}_{j\mathbf{q}}]|0\rangle = U^2[N_{cell} - (N_{i\downarrow} + N_{i\uparrow})]\delta_{ij} = U^2[N_{cell} - N_i]\delta_{ij}, \end{aligned} \tag{25}$$

where indices $i, j = A, B, C$.

If we take the diagonal elements of A_{ij} and sum over i, then we get a much more useful sum-rule

$$A \equiv \int d\omega \sum_i A_{i,i}(\mathbf{q},\omega) = \sum_i \langle 0|[\Delta_{i\mathbf{q}}, \Delta^{\dagger}_{i\mathbf{q}}]|0\rangle = U^2\sum_i [N_{cell} - N_i] = U^2[3N_{cell} - N] \propto -(n-3), \tag{26}$$

where total particle number $N = N_A + N_B + N_c$, partilce number of $i-$th sublattice $N_i = N_{i\uparrow} + N_{i\downarrow}$ and filling factor $n = N/N_{cell}$. It should be emphasized that the above sum-rule of spectral functions is exact, which does not depend on what state the system is. One can use the above sum-rule to check the calculations of various theories.

The above Eq.(26) shows that the integral of spectral functions is proportional to filling factor $n-3$ (relative to the half filling). If the filling factor is half filling ($n-3=0$), the integral of spectral functions is exactly zero. While when filling factor is larger (smaller) than half-filling [particle (hole)-doped case], the integral of spectral functions is negative (positive). Our numerical calculations verify above statements. For example, when the filling is half-filling ($n=3$), we see that the spectral functions are odd functions of frequency and the integral of spectral functions vanishes exactly [see panels (c)(d) of Fig. 4 and panel (c) of Fig. 5]. Panel (d) of Fig. 5 shows the spectral functions for particle-doped case ($n=5$), the weight of negative frequency $\omega < 0$ is dominant, and the integral of spectral functions is negative. The above findings may be useful to distinguish the hole-doped between particle-doped superfluid or superconductor in experiments.

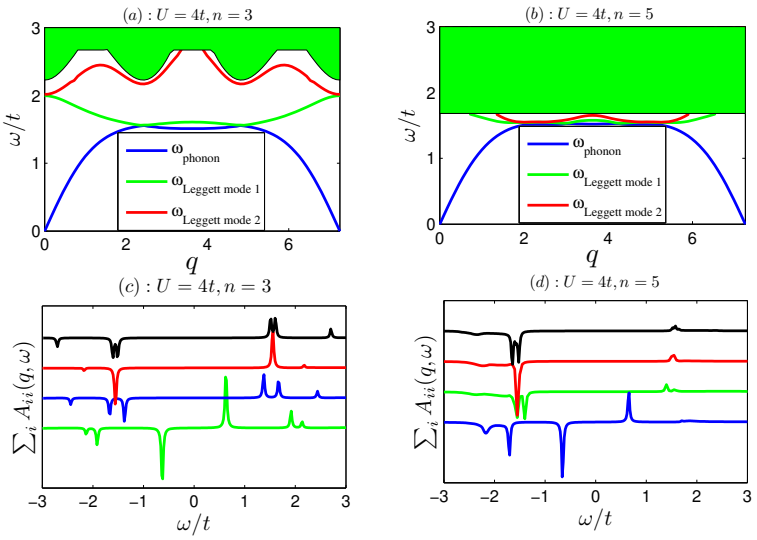

Figure 5. Collective modes [panel (a) and (b)] and two-particle spectral functions [panel (c) and (d)]. (a): The phonon (Leggett) mode is plotted in blue (green and red) lines. The interaction $U = 4$, filling factor $n = 3$ in panel (a). (b): The phonon mode and Leggett modes with $U = 4; n = 5$. (c): Spectral functions with $U = 4; n = 3$. (d): Spectral functions with $U = 4; n = 5$. The spectral functions of $q = 0.5, 1.5, 2.5$ and 3.5 are plotted in blue, green, red and black lines, respectively.

1	2	3	4	5	6	7	8	9
q	ω	A_{11}	A_{12}	A_{22}	$\frac{A_{11}}{\Delta_1^2}$	$\frac{A_{12}}{\Delta_1\Delta_2}$	$\frac{A_{22}}{\Delta_2^2}$	$\frac{A_{12}^2}{A_{11}A_{22}}$
0.01	0.018	1274.5	1618.3	2054.8	2306.5	2318.3	2330.0	1.00002
0.1	0.15	129.4	167.9	217.8	234.2	240.5	247.0	1.0002
0.5	0.66	24.17	34.01	47.82	43.75	48.72	54.22	1.0007

Table 1. The verifications of Eq.(28) and Eq.(30) of spectral functions near the phonon modes with $U = 4$ and filling factor $n = 5$ [$\Delta_1 \simeq 0.7434$ and $\Delta_2 \simeq 0.9391$ same as that in panel (b) and (d) of Fig. 5].

In addition, for a fixed $\mathbf{q}$, when ω approaches some non-degenerate collective modes (e.g., phonon or Leggett modes), from the definition Eq.(19), the spectral functions should take the following forms

$$\begin{aligned} A_{i,i}(\mathbf{q},\omega) &= \langle 0|\Delta_{i\mathbf{q}}|n\rangle\langle n|\Delta_{i\mathbf{q}}^{\dagger}|0\rangle\delta(\omega-\omega_{n0}),\\ A_{i,j}(\mathbf{q},\omega) &= \langle 0|\Delta_{i\mathbf{q}}|n\rangle\langle n|\Delta_{j\mathbf{q}}^{\dagger}|0\rangle\delta(\omega-\omega_{n0}),\\ A_{j,j}(\mathbf{q},\omega) &= \langle 0|\Delta_{j\mathbf{q}}|n\rangle\langle n|\Delta_{j\mathbf{q}}^{\dagger}|0\rangle\delta(\omega-\omega_{n0}), \end{aligned} \tag{27}$$

where $|n\rangle = |\mathbf{q}\rangle$ is wave function of the collective mode, ω_{n0} is its excitation energy. As a result of that, when $\omega \simeq \omega_{n0}$, the heights of peaks of two-particle spectral functions near the collective mode should satisfy a relation, i.e.,

$$|A_{i,j}(\mathbf{q},\omega)|^2 = A_{i,i}(\mathbf{q},\omega)A_{j,j}(\mathbf{q},\omega). \tag{28}$$

When q is small ($q \to 0$), the matrix elements of two-particle Green functions at zero frequency $\omega = 0$ are proportional to product of two order parameters, namely[46]

$$\begin{aligned} G_{II,ij}(\mathbf{q},0) &\simeq -4Z\Delta_i\Delta_j^*,\\ F_{II,ij}(\mathbf{q},0) &\simeq 4Z\Delta_i\Delta_j, \end{aligned} \tag{29}$$

where $Z \equiv \sum_n[\frac{|\langle 0|\hat{\theta}_{\mathbf{q}}|n\rangle|^2}{\omega_{n0}} + \frac{|\langle 0|\hat{\theta}_{-\mathbf{q}}|n\rangle|^2}{\omega_{n0}}] \simeq 1/(q^2\rho_s) > 0$ is a real number and $\hat{\theta}_{\mathbf{q}}$ the phase operator[57,58].

In such a case, it is expected that, for small q, the two-particle spectral functions near the phonon states [$\omega \simeq \omega_{phonon}(\mathbf{q})$ or

$\omega \simeq -\omega_{phonon}(-\mathbf{q})]$ are also proportional to product of superfluid order parameters, i.e.,

$$A_{ij}(\mathbf{q},\omega) \simeq 4Z_{+}\Delta_i\Delta_j^{*}\delta[\omega-\omega_{phonon}(\mathbf{q})] - 4Z_{-}\Delta_i\Delta_j^{*}\delta[\omega+\omega_{phonon}(-\mathbf{q})],$$
$$B_{i,j}(\mathbf{q},\omega) \simeq -4Z_{+}\Delta_i\Delta_j\delta[\omega-\omega_{phonon}(\mathbf{q})] + 4Z_{-}\Delta_i\Delta_j\delta[\omega+\omega_{phonon}(-\mathbf{q})], \tag{30}$$

where $|\mathbf{q}\rangle$ and $|-\mathbf{q}\rangle$ are phonon states with momentum $\mathbf{q}$ and $-\mathbf{q}$, respectively. $Z_{+} = |\langle 0|\hat{\theta}_{\mathbf{q}}|\mathbf{q}\rangle|^2$ and $Z_{-} = |\langle 0|\hat{\theta}_{-\mathbf{q}}|-\mathbf{q}\rangle|^2$ are two real number, which are approximately equal as $q \to 0$.

Our numerical calculations indeed verify Eq.(28) and Eq.(30) for the case of $q \to 0$. For example, some numerical results of spectral functions are listed in TABLE I. It is found that, for extremely small wave vector ($q = 0.01$), both Eq.(28) and Eq.(30) are satisfied approximately . As q increases from $q = 0.01$ to $q = 0.1$ and $q = 0.5$, Eq.(30) becomes invalid gradually (see the columns $6, 7, 8$ in the TABLE I). Nevertheless, Eq.(28) still holds (see the last column of the TABLE I).

Discussion

In conclusion, we investigate the superfluid properties of attractive Hubbard model in dice lattice. The evolution trends of order parameters and superfluid density as functions of filling factors and interactions are analyzed in great detail. We emphasize the special important roles of effective masses in the understanding of the asymptotic behaviors of superfluid density, especially for small filling factor. When both the filling factor and interaction are small, the superfluid density is given by the effective mass of single particle energy band. When interaction is strong, the superfluid density is inversely proportional to interaction, which is also related to effective mass of tightly bound pairs. At strong interaction limit, the asymptotic behavior of superfluid density is captured by a parabola function of filling factor. In addition, the flat band has significant influences on superfluidity. To be specific, the infinite large density of states of flat band results in a linear interaction-dependence of superfluid order parameters. When interaction is weak, the existences of Dirac points and vanishingly small order parameters cause the logarithmic singularity of superfluid density.

Due to the existence of three order parameters, there are three collective modes, i.e., one is the gapless phonon, which corresponds to total density oscillations; the others are gapped Leggett modes, which are characterized by the relative density oscillations between different sublatices. It is found that the undamped Leggett modes can exist in strong interaction cases. In addition, the collective modes can be reflected by sharp peaks in the two-particle spectral functions. The behaviors of two-particle spectral functions near the phonon modes are also analyzed in detail. In addition, an exact sum-rule of spectral functions is derived. For theoretical aspects, the sum-rule can be used to check the various theoretical calculations. In experiments, the sum-rule of the spectral functions may be useful to distinguish the hole-doped or particle-doped superfluid (or superconductor).

Methods

The Hamiltonian Eq.(1) can be solved with the mean-field theory. The superfluid order parameter (pairing gap) $\Delta_{A(B,C)} = -U\langle a(b,c)_{i\downarrow}a(b,c)_{i\uparrow}\rangle$. The Bogoliubov-de Gennes Hamiltonian:

$$\mathscr{H}_{\mathrm{BdG}} = \sum_{\mathbf{k}} \Psi^{\dagger}(\mathbf{k}) H_{\mathrm{BdG}}(\mathbf{k}) \Psi(\mathbf{k}), \tag{31}$$

which $\Psi^{\dagger}(\mathbf{k}) = [a_{\uparrow}^{\dagger}(\mathbf{k}), b_{\uparrow}^{\dagger}(\mathbf{k}), c_{\uparrow}^{\dagger}(\mathbf{k}), a_{\downarrow}(-\mathbf{k}), b_{\downarrow}(-\mathbf{k}), c_{\downarrow}(-\mathbf{k})]$ and

$$H_{\mathrm{BdG}}(\mathbf{k}) = \begin{bmatrix} -\mu & h_{12}(\mathbf{k}) & 0 & \Delta_{\mathrm{A}} & 0 & 0 \\ h_{21}(\mathbf{k}) & -\mu & h_{23}(\mathbf{k}) & 0 & \Delta_{\mathrm{B}} & 0 \\ 0 & h_{32}(\mathbf{k}) & -\mu & 0 & 0 & \Delta_{\mathrm{C}} \\ \Delta_{\mathrm{A}}^{*} & 0 & 0 & +\mu & -h_{12}^{*}(-\mathbf{k}) & 0 \\ 0 & \Delta_{\mathrm{B}}^{*} & 0 & -h_{21}^{*}(-\mathbf{k}) & \mu & -h_{23}^{*}(-\mathbf{k}) \\ 0 & 0 & \Delta_{\mathrm{C}}^{*} & 0 & -h_{32}^{*}(-\mathbf{k}) & +\mu \end{bmatrix}. \tag{32}$$

The Bogoliubov transformation of above equation is readily carried out to obtain the eigenenergies $E^{p(h)1,2,3}(\mathbf{k})$, where $p(h)$ corresponds to the particle (hole) and $1, 2, 3$ represent three branches of energy. The thermodynamic potential per unit cell in the ground state is

$$\Omega = \frac{1}{N_{cell}} \sum_{\mathbf{k}} [-|E^{p1}(\mathbf{k})| - |E^{p2}(\mathbf{k})| - |E^{p3}(\mathbf{k})| - 3\mu] + \frac{(\Delta_{\mathrm{A}}^2 + \Delta_{\mathrm{B}}^2 + \Delta_{\mathrm{C}}^2)}{U}, \tag{33}$$

where N_{cell} is the number of unit cells. The order parameters (or pairing gaps) and chemical potential can be obtained by solving $\partial\Omega/\partial\Delta_{\mathrm{A,B,C}} = 0$, and $n = -\partial\Omega/\partial\mu$ consistently. In the whole paper, we set $t = 1$ as the energy unit and lattice spacing $a = 1$.

References

1. Peotta, S. & Törmä, P. Superfluidity in topologically nontrivial flat bands. *Nat.Commun.* **6**, 8944, DOI: https://doi.org/10.1038/ncomms9944 (2015).
2. Iskin, M. Collective excitations of a bcs superfluid in the presence of two sublattices. *Phys. Rev. A* **101**, 053631, DOI: https://doi.org/10.1103/PhysRevA.101.053631 (2020).
3. Cao, Y. & et.al. Unconventional superconductivity in magic-angle graphene superlattices. *Nature* **556**, 43, DOI: https://doi.org/10.1038/nature26160 (2018).
4. Leggett, A. J. Number-phase fluctuations in two-band superconductors. *Prog.Theor.Phys.* **36**, 901, DOI: https://doi.org/10.1143/PTP.36.901 (1966).
5. Iskin, M. & Sáde Melo, C. A. R. Bcs-bec crossover of collective excitations in two-band superfluids. *Phys. Rev. B* **72**, 024512, DOI: https://doi.org/10.1103/PhysRevB.72.024512 (2005).
6. He, L., Wang, J., Peng, S.-G., Liu, X.-J. & Hu, H. Strongly correlated fermi superfluid near an orbital feshbach resonance: Stability, equation of state, and leggett mode. *Phys. Rev. A* **94**, 043624, DOI: https://doi.org/10.1103/PhysRevA.94.043624 (2016).
7. Zhang, Y.-C., Ding, S. & Zhang, S. Collective modes in a two-band superfluid of ultracold alkaline-earth-metal atoms close to an orbital feshbach resonance. *Phys. Rev. A* **95**, 041603(R), DOI: https://doi.org/10.1103/PhysRevA.95.041603 (2017).
8. Klimin, S. N., Kurkjian, H. & Tempere, J. Leggett collective excitations in a two-band fermi superfluid at finite temperatures. *New J. Phys.* **21**, 113043, DOI: https://iopscience.iop.org/article/10.1088/1367-2630/ab54b0/meta (2019).
9. Honerkamp, C. & Hofstetter, W. Ultracold fermions and the su(n) hubbard model. *Phys. Rev. Lett.* **92**, 170403, DOI: https://doi.org/10.1103/PhysRevLett.92.170403 (2004).
10. Rapp, A., Zaránd, G., Honerkamp, C. & Hofstetter, W. Color superfluidity and baryon formation in ultracold fermions. *Phys. Rev. Lett.* **98**, 160405, DOI: https://doi.org/10.1103/PhysRevLett.98.160405 (2007).
11. Liu, X.-J., Hu, H. & Drummond, P. D. Multicomponent strongly attractive fermi gas: A color superconductor in a one-dimensional harmonic trap. *Phys. Rev. A* **77**, 013622, DOI: https://doi.org/10.1103/PhysRevA.77.013622 (2008).
12. Cherng, R. W., Refael, G. & Demler, E. Superfluidity and magnetism in multicomponent ultracold fermions. *Phys. Rev. Lett.* **99**, 130406, DOI: https://doi.org/10.1103/PhysRevLett.99.130406 (2007).
13. Kanász-Nagy, M. & Zaránd, G. Global superfluid phase diagram of a three-component fermion mixture with magnetic ordering. *Phys. Rev. B* **86**, 064519, DOI: https://doi.org/10.1103/PhysRevB.86.064519 (2012).
14. Martikainen, J.-P., Kinnunen, J. J., Törmä, P. & Pethick, C. J. Induced interactions and the superfluid transition temperature in a three-component fermi gas. *Phys. Rev. Lett.* **103**, 260403, DOI: https://doi.org/10.1103/PhysRevLett.103.260403 (2009).
15. Zhu, Q., Zhang, C. & Wu, B. Exotic superfluidity in spin-orbit coupled bose-einstein condensates. *Eur. Lett.* **100**, 50003, DOI: https://iopscience.iop.org/article/10.1209/0295-5075/100/50003/meta (2012).
16. Hazra, T., Verma, N. & Randeria, M. Bounds on the superconducting transition temperature: Applications to twisted bilayer graphene and cold atoms. *Phys. Rev. X* **9**, 031049, DOI: https://doi.org/10.1103/PhysRevX.9.031049 (2019).
17. Julku, A., Peotta, S., Vanhala, T. I., Kim, D.-H. & Törmä, P. Geometric origin of superfluidity in the lieb-lattice flat band. *Phys. Rev. Lett.* **117**, 045303, DOI: https://doi.org/10.1103/PhysRevLett.117.045303 (2016).
18. Julku, A., Peltonen, T. J., Liang, L., Heikkilä, T. T. & Törmä, P. Superfluid weight and berezinskii-kosterlitz-thouless transition temperature of twisted bilayer graphene. *Phys. Rev. B* **101**, 060505(R), DOI: https://doi.org/10.1103/PhysRevB.101.060505 (2020).
19. Liang, L. & et.al. Band geometry, berry curvature, and superfluid weight. *Phys. Rev. B* **95**, 024515, DOI: https://doi.org/10.1103/PhysRevB.95.024515 (2017).
20. Hu, X., Hyart, T., Pikulin, D. I. & Rossi, E. Geometric and conventional contribution to the superfluid weight in twisted bilayer graphene. *Phys. Rev. Lett.* **123**, 237002, DOI: https://doi.org/10.1103/PhysRevLett.123.237002 (2019).
21. Xie, F., Song, Z., Lian, B. & Bernevig, B. A. Topology-bounded superfluid weight in twisted bilayer graphene. *Phys. Rev. Lett.* **124**, 167002, DOI: https://doi.org/10.1103/PhysRevLett.124.167002 (2020).
22. Provost, J. P. & Vallee, G. Riemannian structure on manifolds of quantum states. *Commun. Math. Phys.* **76**, 289, DOI: https://doi.org/10.1007/BF02193559 (1980).

23. Sutherland, B. Localization of electronic wave functions due to local topology. *Phys. Rev. B* **34**, 5208, DOI: https://doi.org/10.1103/PhysRevB.34.5208 (1986).

24. Vidal, J., Mosseri, R. & Doucot, B. Aharonov-bohm cages in two-dimensional structures. *Phys. Rev. Lett.* **81**, 5888, DOI: https://doi.org/10.1103/PhysRevLett.81.5888 (1998).

25. Gorbar, E. V., Gusynin, V. P. & Oriekhov, D. O. Electron states for gapped pseudospin-1 fermions in the field of a charged impurity. *Phys. Rev. B* **99**, 155124, DOI: https://doi.org/10.1103/PhysRevB.99.155124 (2019).

26. B., D., Kailasvuori, J. & Moessner, R. Lattice generalization of the dirac equation to general spin and the role of the flat band. *Phys. Rev. B* **84**, 195422, DOI: https://doi.org/10.1103/PhysRevB.84.195422 (2011).

27. Xu, H.-Y. & Lai, Y.-C. Anomalous chiral edge states in spin-1 dirac quantum dots. *Phys. Rev. Res.* **2**, 013062, DOI: https://doi.org/10.1103/PhysRevResearch.2.013062 (2020).

28. Wang, F. & Ran, Y. Nearly flat band with chern number c=2 on the dice lattice. *Phys. Rev. B* **84**, 241103(R), DOI: https://doi.org/10.1103/PhysRevB.84.241103 (2011).

29. Bercioux, D., Urban, D. F., Grabert, H. & Häusler, W. Massless dirac-weyl fermions in a t_3 optical lattice. *Phys. Rev.A* **80**, 063603, DOI: https://doi.org/10.1103/PhysRevA.80.063603 (2009).

30. Illes, E. & Nicol, E. J. Magnetic properties of the $\alpha - t_3$ model: Magneto-optical conductivity and the hofstadter butterfly. *Phys. Rev. B* **94**, 125435, DOI: https://doi.org/10.1103/PhysRevB.94.125435 (2016).

31. Chen, Y.-R., Xu, Y., Wang, J., Liu, J.-F. & Z., M. Enhanced magneto-optical response due to the flat band in nanoribbons made from the $\alpha - t_3$ lattice. *Phys. Rev. B* **99**, 045420, DOI: https://doi.org/10.1103/PhysRevB.99.045420 (2019).

32. Illes, E. & Nicol, E. J. Klein tunneling in the $\alpha - t_3$ model. *Phys. Rev. B* **95**, 235432, DOI: https://doi.org/10.1103/PhysRevB.95.235432 (2017).

33. Biswas, T. & Ghosh, T. K. Dynamics of a quasiparticle in the $\alpha - t_3$ model: role of pseudospin polarization and transverse magnetic field on zitterbewegung. *J. Phys.: Condens. Matter* **30**, 075301, DOI: https://doi.org/10.1103/PhysRevB.95.235432? (2018).

34. Raoux, A., Morigi, M., Fuchs, J.-N., Piéchon, F. & Montambaux, G. From dia- to paramagnetic orbital susceptibility of massless fermions. *Phys. Rev. Lett.* **112**, 026402, DOI: https://doi.org/10.1103/PhysRevLett.112.026402 (2014).

35. Biswas, T. & Ghosh, T. Magnetotransport properties of the $\alpha - t_3$ model. *J. Physics: Condens. Matter* **28**, 495302, DOI: https://doi.org/10.1103/PhysRevLett.112.026402? (2016).

36. Islam, S. F. & Dutta, P. Valley-polarized magnetoconductivity and particle-hole symmetry breaking in a periodically modulated $\alpha - t_3$ lattice. *Phys. Rev. B* **96**, 045418, DOI: https://doi.org/10.1103/PhysRevB.96.045418 (2017).

37. Blumberg, G. & et al. Observation of leggett's collective mode in a multi-band mgb_2 superconductor. *Phys. Rev. Lett.* **99**, 227002, DOI: https://doi.org/10.1103/PhysRevLett.99.227002 (2007).

38. Mou, D. & et al. Strong interaction between electrons and collective excitations in the multiband superconductor mgb_2. *Phys. Rev. B* **91**, 140502(R), DOI: https://doi.org/10.1103/PhysRevB.91.140502 (2015).

39. Zhang, Y.-C., Xu, Z. & Zhang, S. Topological superfluids and the bec-bcs crossover in the attractive haldane-hubbard model. *Phys. Rev. A* **95**, 043640, DOI: https://doi.org/10.1103/PhysRevB.95.043640 (2017).

40. Heiselberg, H. Crossovers in unitary fermi systems, bcs-bec crossover and the unitary fermi gas, edited by w. zwerger (Springer, Berlin, 2017).

41. Iglovikov, V. I., Hébert, F., Grémaud, B., Batrouni, G. G. & Scalettar, R. T. Superconducting transitions in flat-band systems. *Phys. Rev. B* **90**, 094506, DOI: https://doi.org/10.1103/PhysRevB.90.094506 (2014).

42. Wu, C. & Sarma, S. D. $p_{x,y}$-orbital counterpart of graphene: Cold atoms in the honeycomb optical lattice. *Phys. Rev. B* **77**, 235107, DOI: https://doi.org/10.1103/PhysRevB.77.235107 (2008).

43. Zhang, S., Hung, H.-h. & Wu, C. Proposed realization of itinerant ferromagnetism in optical lattices. *Phys. Rev. A* **82**, 053618, DOI: https://doi.org/10.1103/PhysRevA.82.053618 (2010).

44. Kopnin, N. B., Heikkila, T. T. & Volovik, G. E. High-temperature surface superconductivity in topological flat-band systems. *Phys. Rev. B* **83**, 220503(R), DOI: https://doi.org/10.1103/PhysRevB.83.220503(R) (20011).

45. Fisher, M. E., Barber, M. N. & Jasnow, D. Helicity modulus, superfluidity, and scaling in isotropic systems. *Phys. Rev. A* **8**, 1111, DOI: https://doi.org/10.1103/PhysRevA.8.1111 (1973).

46. Zhang, Y.-C. Superfluid density, josephson relation and pairing fluctuations in a multi-component fermion superfluid. *arXiv:* **2012**, 11217, DOI: https://arXiv:2012.11217 (2020).

47. Pieri, P. & Strinati, G. C. Strong-coupling limit in the evolution from bcs superconductivity to bose-einstein condensation. *Phys. Rev. B* **61**, 15370, DOI: https://doi.org/10.1103/PhysRevB.61.15370 (2000).

48. Zhang, Y. C. & et.al. Superfluid density of a spin-orbit-coupled bose gas. *Phys. Rev. A* **94**, 033635, DOI: https://doi.org/10.1103/PhysRevA.94.033635 (2016).

49. Zhang, Y. C., Wang, H. T., Shen, S. Q. & Liu, W. M. Particle-hole bound states of dipolar molecules in optical lattice. *Chin. Phys. B* **22**, 090501, DOI: https://iopscience.iop.org/article/10.1088/1674-1056/22/9/090501/meta (2013).

50. Onogi, T. & Murayama, Y. Two-dimensional superfluidity and localization in the hard core boson model: A quantum monte carlo study. *Phys. Rev. B* **49**, 9009, DOI: https://doi.org/10.1103/PhysRevB.49.9009 (1994).

51. Micnas, R., Robaszkiewicz, S. & Kostyrko, T. Thermodynamic and electromagnetic properties of hard-core charged bosons on a lattice. *Phys. Rev. B* **52**, 6863, DOI: https://doi.org/10.1103/PhysRevB.52.6863 (1995).

52. Engelbrecht, J. R., Randeria, M. & Sáde Melo, C. A. R. Bcs to bose crossover: Broken-symmetry state. *Phys. Rev. B* **55**, 15153, DOI: https://doi.org/10.1103/PhysRevB.55.15153 (1997).

53. Hu, H., Liu, X.-J. & Drummond, P. D. Equation of state of a superfluid fermi gas in the bcs-bec crossover. *Eur. Lett.* **74**, 574, DOI: https://iopscience.iop.org/article/10.1209/epl/i2006-10023-y/meta (2006).

54. Diener, R. B., Sensarma, R. & Randeria, M. Quantum fluctuations in the superfluid state of the bcs-bec crossover. *Phys. Rev. A* **77**, 023626, DOI: https://doi.org/10.1103/PhysRevA.77.023626 (2008).

55. Samanta, A., Ratnakar, A., Trivedi, N. & Sensarma, R. Two-particle spectral function for disordered s-wave superconductors: Local maps and collective modes. *Phys. Rev. B* **101**, 024507, DOI: https://doi.org/10.1103/PhysRevB.101.024507 (2020).

56. White, S. R. Spectral weight function for the two-dimensional hubbard model. *Phys. Rev. B* **44**, 4670, DOI: https://doi.org/10.1103/PhysRevB.44.4670 (1991).

57. Zhang, Y.-C. Generalized josephson relation for conserved charges in multicomponent bosons. *Phys. Rev. A* **98**, 033611, DOI: https://doi.org/10.1103/PhysRevA.98.033611 (2018).

58. Lifshitz, E. M. & Pitaevskii, L. P. Statistical physics part 2. Academic, London (1980).

Acknowledgements (not compulsory)

Y. R. W. and Y.C. Z. are supported by the NSFC under Grants No.11874127 and startup grant from Guangzhou University. X.F.Z. is Supported by the National Natural Science Foundation of China (Grant No. 11775253) and the Key Research Program of Frontier Sciences, CAS under Grant No. ZDBS-LY-7016. C. F. L. is supported by the NSFC under grant Nos. 11875149 and 61565007, The Youth Jinggang Scholars Program in Jiangxi Province, and The Program of Qingjiang Excellent Yong Talents, Jiangxi University of Science and Technology. W.M. L. is supported by the National Key R&D Program of China under grants No. 2016YFA0301500, NSFC under grants Nos.11434015, 61227902.

Author contributions statement

Y.R W. and Y.C.Z. performed calculations. Y.R W., X.F.Z., C.F.L., W.M.L., and Y.C.Z. analyzed numerical results. Y.R W., X.F.Z., C.F.L., W.M.L., and Y.C.Z. contributed in completing the paper.

Additional information

Competing interests: The authors declare no competing interests

The corresponding author is responsible for submitting a competing interests statement on behalf of all authors of the paper.

Figures

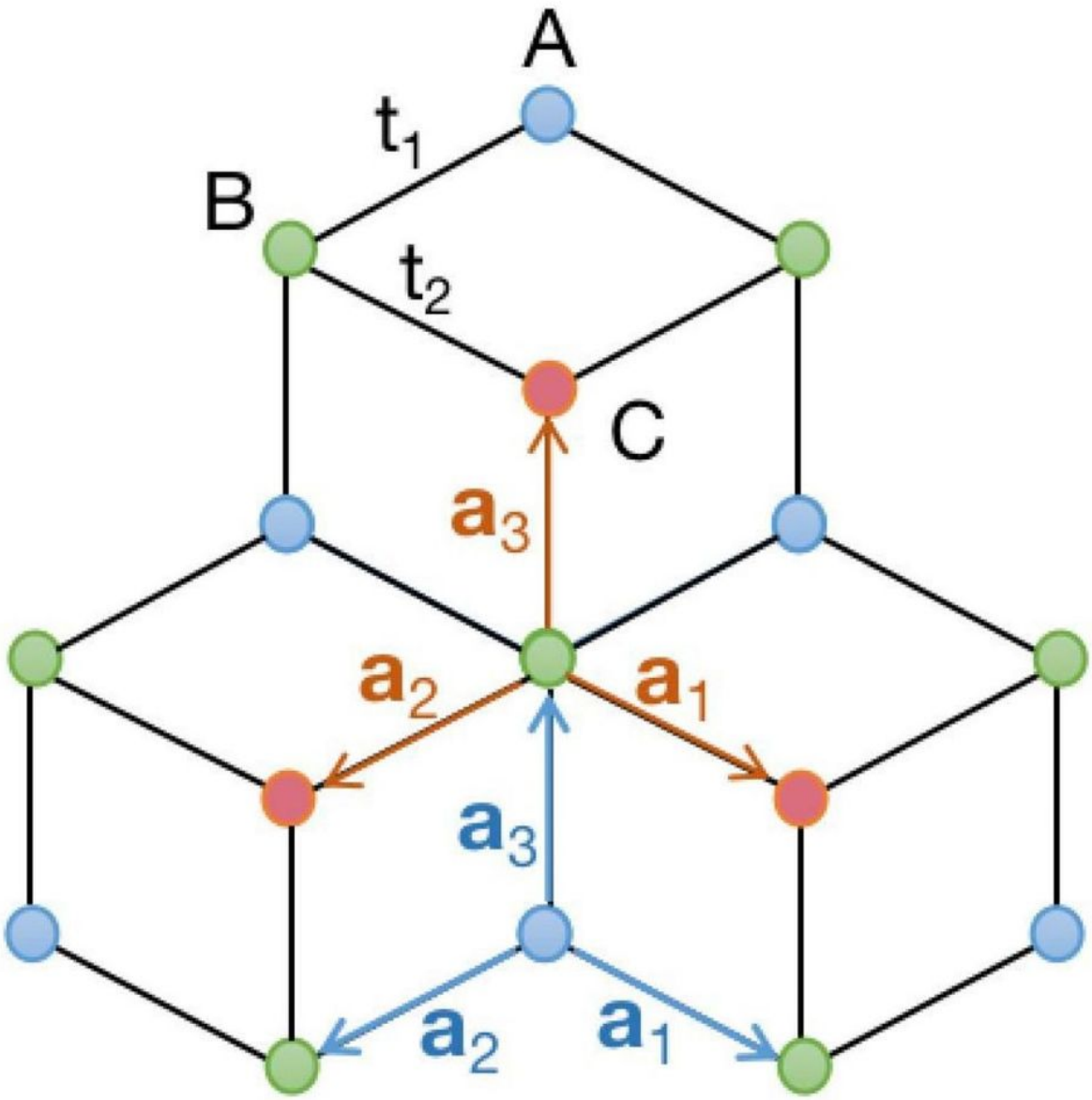

Figure 1

Please see the Manuscript PDF file for the complete figure caption

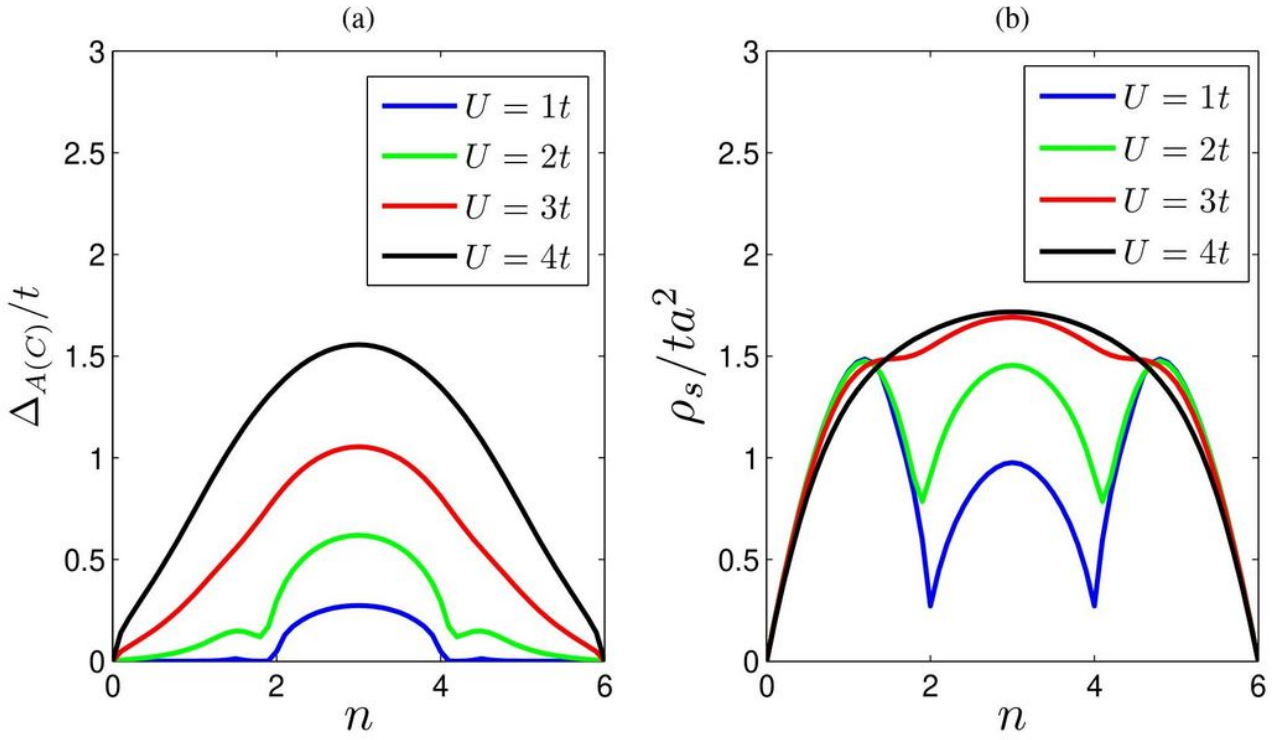

Figure 2

Please see the Manuscript PDF file for the complete figure caption

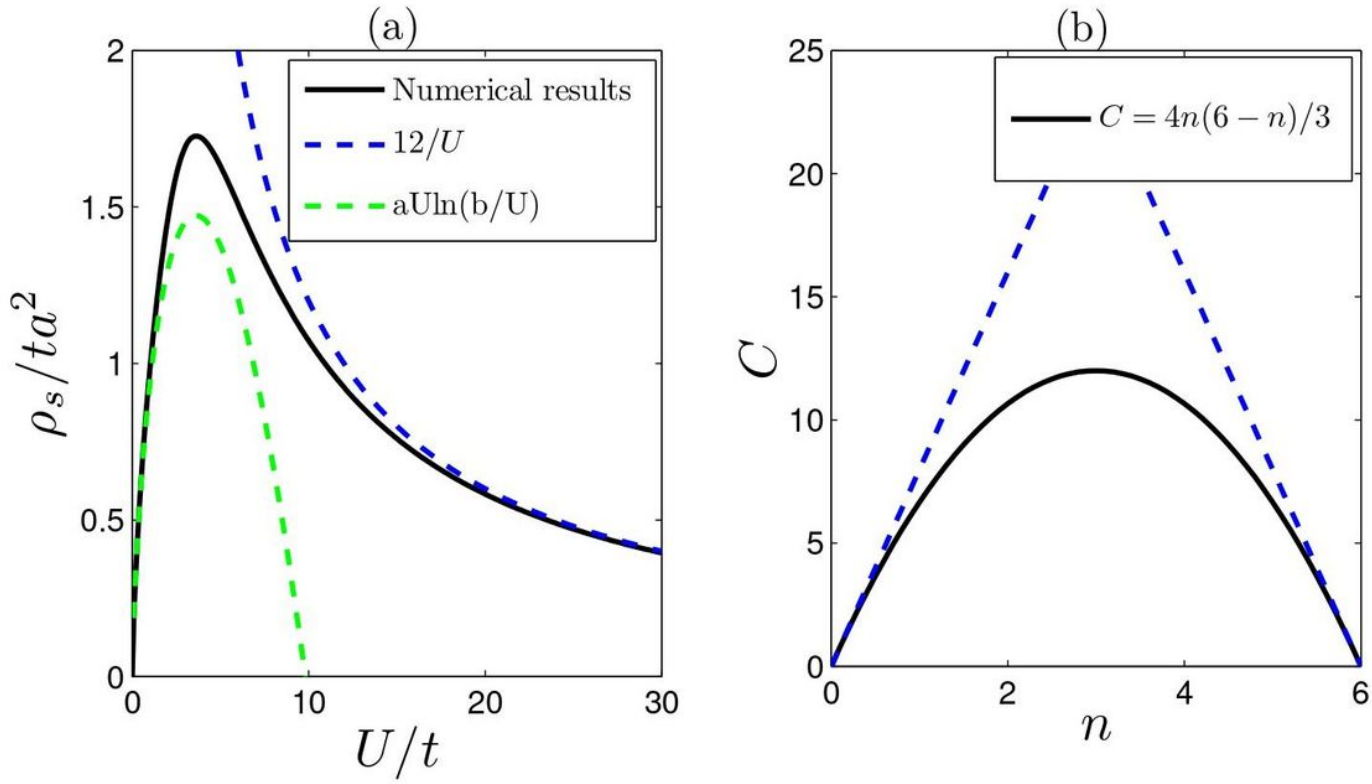

Figure 3

Please see the Manuscript PDF file for the complete figure caption

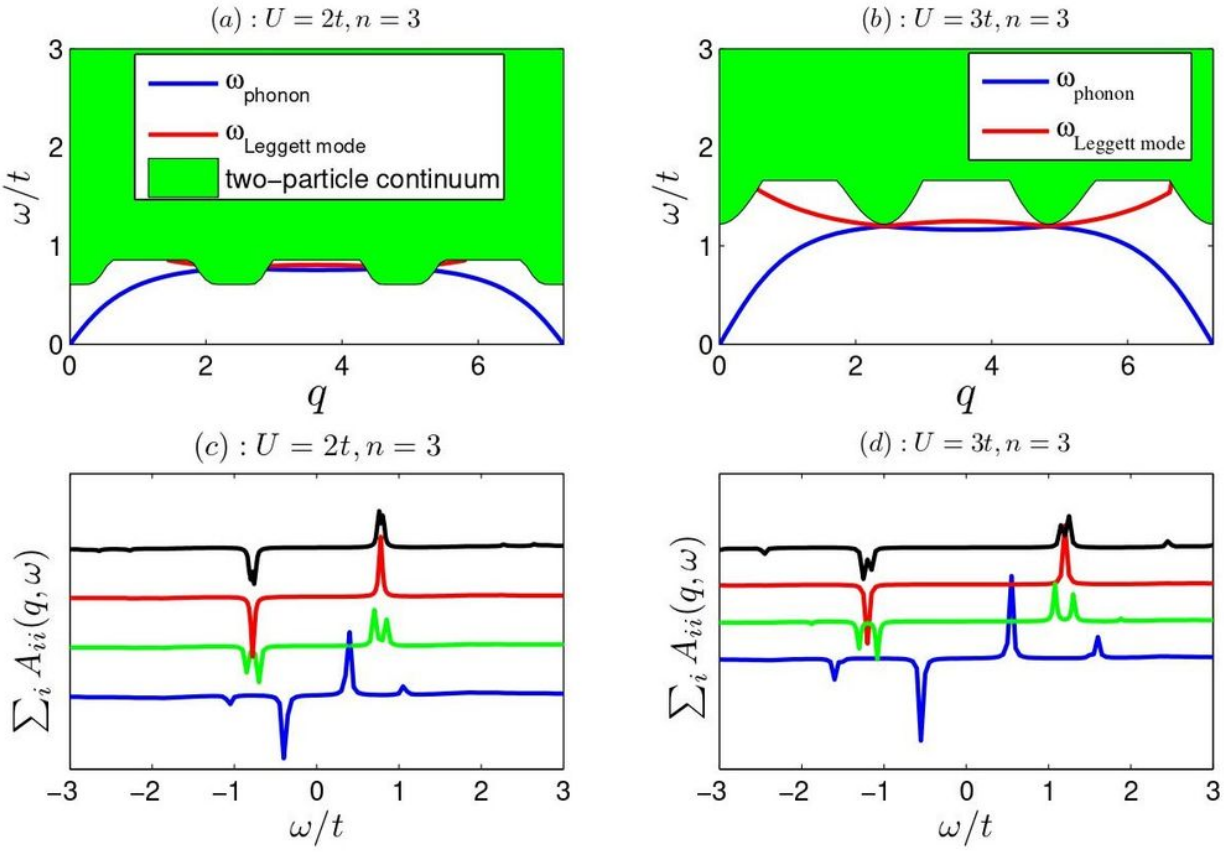

Figure 4

Please see the Manuscript PDF file for the complete figure caption

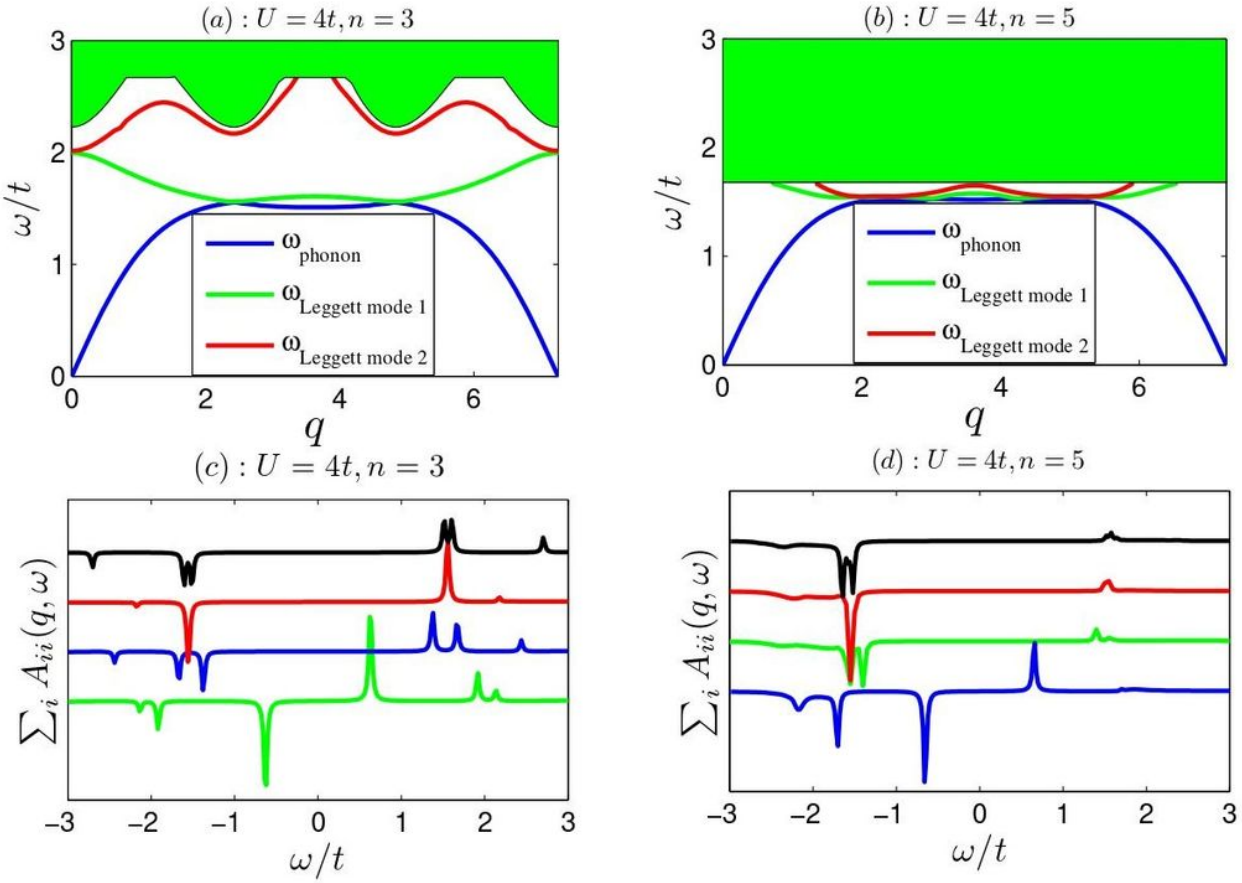

Figure 5

Please see the Manuscript PDF file for the complete figure caption